VALIDATION OF A COUPLED THERMAL-HYDROLOGICAL-MECHANICAL MODEL THROUGH A COMPARATIVE STUDY OF SHEAR STIMULATION IN TWO GEOTHERMAL ENVIRONMENTS: USA AND NEW ZEALAND

David Dempsey[1], Jonathon Clearwater[2], Sharad Kelkar[1] and Irene Wallis[2]

[1]Los Alamos National Laboratory, Los Alamos, New Mexico, USA

[2]Mighty River Power Ltd., PO Box 245, Rotorua 3010, New Zealand

d.dempsey@lanl.gov

Keywords: *Geothermal, injectivity, stimulation, numerical model, coupled flow-stress, permeability.*

ABSTRACT

Injection of cold water has been demonstrated to improve injectivity at Desert Peak EGS well 27-15, Nevada, as well as numerous wells at Ngatamariki and other New Zealand geothermal fields. The injectivity index (II) of a well is generally observed to evolve according to a power law – i.e., $II \propto t^n$, where the exponent n ranges between 0.3 and 0.7. Conceptually, injectivity gain is attributed to the creation of a stimulated volume of either shear-enhanced fracture permeability or thermal contraction of matrix rock in a confined aquifer.

In earlier work, a coupled thermo-hydro-mechanical model was constructed for the 2010 Desert Peak EGS shear stimulation. Here, we further validate that model through its application to a 30-day cold-water injection stimulation of a well in the Ngatamariki geothermal field. The model calculates anisotropic permeability enhancement as a function of thermal and pressure induced Mohr-Coulomb shear failure; only the reactivation of existing fractures is considered – not the creation of new ones. Applied to Desert Peak, the model matched an observed 15-fold increase in II with n = 0.33 and suggested that a spherical stimulation zone had been created. In this study we extend the model to conditions appropriate for the Ngatamariki field. Both fields are located within an extensional stress regime; however, Ngatamariki exhibits much higher initial permeability, greater fracture density and more anisotropy in fracture orientations than observed at Desert Peak.

In contrast to Desert Peak, during the stimulation of a Ngatamariki well, an 8-fold increase in injectivity was observed with $n =$ 0.62. Comparisons between such disparate datasets improve our understanding of injectivity evolution and its connection to changes in the reservoir. For example, a model for the Ngatamariki stimulation indicates that the damaged zone is more planar than at Desert Peak; this may represent stimulation of a single fracture or narrow fracture zone. More generally, sensitivity analysis indicates that Desert Peak and Ngatamariki represent two end-members of a more general relationship between n and stimulation geometry.

1. INTRODUCTION

Well injectivity, which quantifies the injected flow rate in terms of the down-hole and reservoir pressure difference, is a useful measure of injection well performance. Stimulation of geothermal wells to improve injectivity can be achieved by the injection of light acid, high pressure water to create and grow hydraulic fractures, or cold-water injection at medium to low pressure. The latter approach aims to improve the permeability of existing fractures by increasing their hydraulic aperture. This is achieved by increasing pore pressure and thermal contraction of the fracture walls upon cooling – an elastic phenomenon - which can induce self-propping shear failure on the fracture, i.e., a plastic deformation. Note that there will be some reversible permeability enhancement (Grant et al., 2013) resulting from the elastic component of rock deformation; however, induced shear displacements on fractures are irreversible (although permeability decreases due to chemical sealing and healing may be observed in the longer term).

Grant et al. (2013) provide a case review of thermal stimulation in New Zealand and Iceland geothermal fields. They describe observations that the injectivity of geothermal wells improves with continued injection; this gain can be partly reversed during episodes of production. Furthermore, the time evolution of injectivity, II, is generally linear under log-log transformation, i.e., $II \propto t^n$; observations indicate n ranges between 0.3 and 0.7 (Grant et al., 2013; Dempsey et al., 2013).

Shear stimulation was undertaken as part of a multi-faceted stimulation operation of well 27-15 at the Desert Peak geothermal field in Nevada (Chabora et al., 2012). Cold-water injection at four well head pressures (WHP), all below the minimum horizontal principal stress, σ_h, resulted in a 15-fold increase of initial injectivity of 0.15 kg s^{-1} MPa^{-1} (0.05 tph bar^{-1}). In this case, permeability enhancement was attributed to self-propping shear failure of an ensemble of existing fractures. A numerical model was constructed that approximately matched injectivity evolution (n=0.33) during the stimulation (Dempsey et al., 2013); the model suggests the formation of a spherical zone of cooled, damaged rock.

In contrast to the Desert Peak experience, thermal stimulations in NZ geothermal fields generally indicate injectivity improvement at higher exponents, e.g., n ~ 0.6-0.7 for Mokai and Ngatamariki (Grant et al., 2013). These fields generally exhibit higher initial injectivity (1 to 10 tph bar^{-1}) and lower relative gains (2- to 5-fold increases). Grant et al. (2013) propose an analytical model of a confined aquifer with increasing permeability attributed to thermal contraction of the rock either side. This model suggests n = 0.5 – 1.5 depending on assumptions regarding the aperture-permeability relationship and flow regime.

In this paper, we investigate the dependence of the injectivity exponent, n, on the geometry of the stimulated region. At Desert Peak, a spherical stimulation volume is modelled and attributed to a relatively isotropic distribution of fracture orientations (Dempsey et al., 2013). For the Ngatamariki well, a higher degree of anisotropy, contributing to formation of a flattened ellipsoidal damage zone, may account for the higher value of n.

2. SITE AND STIMULATION OVERVIEWS

Construction of a numerical model for well stimulation requires initial characterization of the formation material properties, its fractures and the in situ stress, temperature and pressure conditions near the injection well. For the stimulation, estimates of WHP, injection temperature and the time periods they are applied are required.

2.1 Desert Peak, Nevada, USA

Desert Peak is a high-enthalpy, blind geothermal system in western Nevada. The field is coincident with a left-step in the NNE-trending, WNW-dipping Rhyolite Ridge normal fault zone (Faulds et al., 2010); this structure is assumed to supply sub-vertical permeable pathways for hot fluids to ascend from depth. The strike and mode of faulting suggest a minimum horizontal principal stress, σ_h, oriented in the WNW direction (Fig. 1A); this is supported by borehole image log analysis of drilling-induced tensile fractures in well 27-15 that suggests a σ_h azimuth of 114±17° (Davatzes and Hickman, 2009). Hydraulic fracturing tests indicate the magnitude of σ_h is ~0.61 of the vertical stress, σ_v (Hickman and Davatzes, 2010).

The stimulation target was a moderately porous, siliceous rhyolite unit located at a depth of 920 to 1070 m. Physical properties of this lithotype were determined from mechanical testing on core samples (Lutz et al., 2010).

Pre-stimulation temperature profiles indicate temperatures of 190°C at the target depth. Pressure is assumed hydrostatic below a water table 116 m below the ground surface.

Shear stimulation took place at four applied WHPs: 1.5, 2.2, 3.1 and 3.7 MPa. The majority of the injectivity improvement took place during the 35-day 3.1 MPa pressure step. Injectivity started to increase ~6 days after injection began, starting at 0.15 and eventually reaching 1.5 kg s^{-1} MPa^{-1}. Following a 50-day shut-in, stimulation recommenced at the higher WHP of 3.7 MPa; at this time, it was noted that injectivity had declined by approximately a factor of 2.

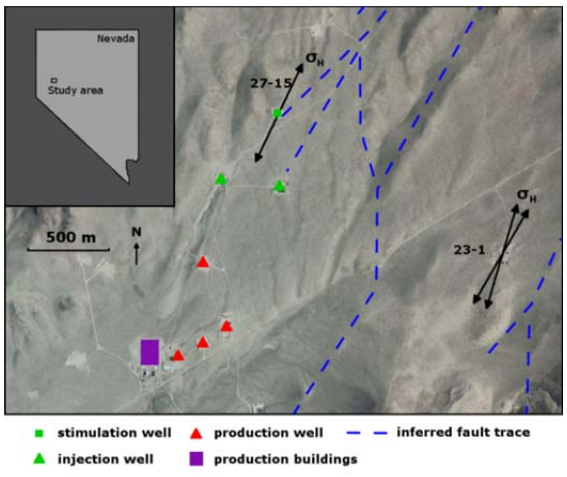

Figure 1A: Summary of infrastructure, inferred structures and stress state at Desert Peak geothermal field (from Dempsey et al., 2013). Stimulation took place at well 27-15.

2.2 Ngatamariki, NZ

Ngatamariki Geothermal Field is located in the central-eastern portion of the Taupo Volcanic Zone (TVZ), which is in turn a zone of active rifting resulting from the oblique subduction of the Pacific Plate under the North Island (Rowland and Sibson, 2004). Ngatamariki is located in a normal faulting environment ($\sigma_V = \sigma_1$: σ_H = 30↔210°) with a high fracture orientation anisotropy, such that nearly all imaged faults and fractures align with the overall trend NE-SW structural trend of the TVZ (Fig. 1B).

Mean fracture density at Ngatamariki varies depending on lithology and the overprinting alteration (Halwa et al., this volume). Considering only those fractures which were interpreted as potentially open at the time of imaging, we found that tuffs, ignimbrites and volcaniclastic deposits typically have a mean fracture density of 1-2 fractures per meter. This contrasts with the intrusive and extrusive lavas, and those tuffs adjacent the intrusive containing significant phillic alteration, which have mean fracture densities between 5 and 7 fractures per meter.

In 2011-2013 development drilling was undertaken at Ngatamariki Geothermal Field for an 82 MW binary plant. One producer and three deep injection wells were drilled. Other injection wells in New Zealand geothermal fields have shown promising stimulation in response to cool water injection (Grant et al., 2013). Accordingly, after completion testing, the Ngatamariki injection wells were injected with 20°C river water to improve well injectivity. The rate of stimulation was quantified in order to predict how injection capacity might evolve in response to plant commissioning. Wells were stimulated with river water for as long as possible (ranging from 19 to 31 days) given operational constraints on water availability. Subsequent to data availability, further work will look at the comparison of well stimulation with river water and well stimulation with brine injection during plant operation.

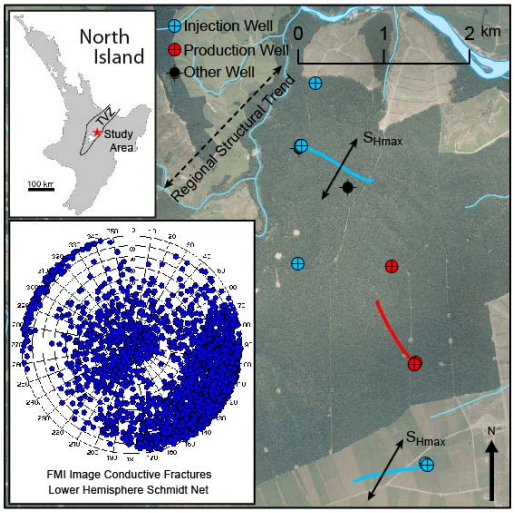

Figure 1B: Summary of infrastructure, regional structural trend and stress state at Ngatamariki geothermal field. The steronet plots poles to plane of all fractures interpreted as potentially open in one well. This density and anisotropy is representative of the field-wide trend.

Grant et al. (2013) report injectivity response during stimulation of one such Ngatamariki injection well. Over a 30-day period, injectivity rose from an initial value of ~1 to between 7 and 8 kg s^{-1} MPa^{-1}. In contrast to Desert Peak, injectivity gains were observed after only one day of injection. This could be attributed to a variety of factors,

including: (i) closer proximity of the stress state to criticality, (ii) weaker fractures, e.g., lower friction coefficient, cohesion, or (iii) operation at higher flow rates facilitating more rapid cooling of the rock.

3. NUMERICAL MODEL

The model of stimulation used in this work has previously been described in Dempsey et al. (2013); only an overview of its components and operation are provided here.

Stimulation is modelled using the code Finite Element Heat and Mass transfer (FEHM) developed at Los Alamos National Laboratory for subsurface fluid flow and coupled stress applications (Zyvoloski, 2007). FEHM solves mass, energy and force balance equations for multi-phase, multi-fluid Darcy flow. Various couplings between the stress and flow solutions can be invoked including: (i) thermal coupling via the coefficient of thermal expansion, (ii) pressure coupling via the Biot coefficient, and (iii) permeability as an arbitrary function of temperature, pressure and stress.

The model is centred on the injection interval and large enough to account for temperature, pressure and stress changes in the near wellbore region. Injection occurs by assigning a fixed overpressure – corresponding to the applied WHP – at the injection site. Mass flow into the model is proportional to the pressure difference between the well and the reservoir.

Injectivity index is defined as flow rate, Q, divided by the pressure difference in the well, P_{DHP}, and the formation, P_{RES}, i.e., $II = Q/(P_{DHP} - P_{RES})$. In this work, the applied WHP is taken as a proxy for the pressure difference. If there is no change of injectivity, the injection rate should be observed to decline from an initial maximum as pressure near the wellbore increases. Thus, flow rate decreases due to conditions in the reservoir. However, during stimulation, flow rates are observed to increase, in spite of a fixed WHP; clearly changes must be occurring in the permeability distribution. Permeability modification is attributed to changes in the stress field and in the code must be calculated as an explicit function of stress.

3.1 Stress-permeability relationship

Our conceptual model is based on stimulation of existing fractures – not the creation of new ones. Injection has four consequences for the in-situ stress state: (i) compressive stresses drop with temperature, i.e., thermal contraction; (ii) compressive stress increases with pressure increase in the rock matrix according to the Biot coupling; (iii) reduction in the effective normal stress on fractures due to an increase in the fluid pressure within the fractures; and (vi) thermal contraction propagates beyond the temperature front as rock at medium distances expands in response to the decompression. Thus, at each time step there is a new stress state in the model; permeability is updated according to the following algorithm.

1. At the beginning of the simulation, a hypothetical fracture population is created and assigned to each block. Fractures can have different orientations but otherwise have identical properties and are equally well connected to each other. Properties of the fracture distribution are detailed in Section 3.2.

2. For each fracture, at each timestep, shear and normal stresses are calculated on the fracture plane and the Mohr-Coulomb failure criterion is assessed

$$\tau > \mu(\sigma_n - p_f) + C, \qquad (1)$$

where τ and σ_n are the shear and normal stress, p_f is the pore fluid pressure, and μ and C are the coefficient of friction and cohesion of the fracture.

3. If failure occurs, a stress drop is calculated using the dynamic friction coefficient. The stress drop is converted to a shear displacement according to a shear stiffness parameter.

4. Permeability on the fracture is increased as a function of the calculated shear displacement. Fracture permeability is ramped to a user-specified maximum. In this work, the permeability-displacement relationship is constrained by laboratory experiments on fractures in granite and marble (Lee and Cho, 2002). Importantly, permeability increases on the fracture plane only.

5. The new permeability for each block is taken as the ensemble average of permeabilities of all fractures. Therefore, if only a subset of specifically oriented fractures fails, permeability enhancement will be anisotropic.

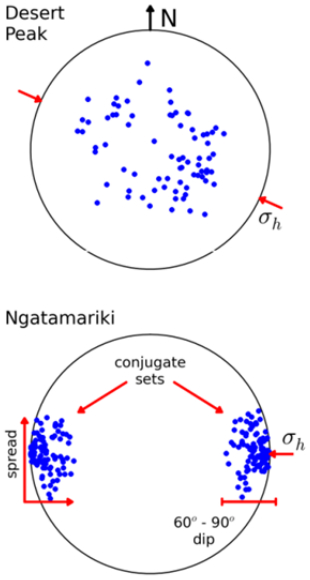

Figure 2: Distribution of measured Desert Peak fracture orientations (Davatzes and Hickman, 2010) and the synthetic distribution used for the Ngatamariki simulation. Labelled features are referred to in the text. The orientation of σ_h is indicated.

3.2 Fracture distributions

The code generates synthetic fracture populations from existing data using a density sampling algorithm. For Desert Peak, fracture orientations for the stimulated well were measured prior to stimulation (Davatzes and Hickman, 2009).

Due to limitations on data availability, we will use assumed fracture distributions for Ngatamariki that are consistent with our hypothesis that the injectivity behavior is related to a higher degree of fracture anisotropy. The distributions have the following properties (see Fig. 2): (i) comprised of two conjugate sets; (ii) the horizontal component of the mean fracture normal is aligned with the minimum horizontal principal stress, σ_h; (iii) fractures dip between 60° and vertical; and (iv) some spread is associated with each set.

Table 1. Parameters for numerical model. Where different, parameters for the Ngatamariki model are provided in brackets.

Parameter	Value
Operational	
Injection depth	1000 m
Injection pressure	3.1 MPa
Injection temperature[1]	100°C
Material	
Thermal conductivity	2.2 W m^{-1} K^{-1}
Density	2480 kg m^{-3}
Specific heat capacity	1200 J m^{-3} K^{-1}
Porosity	0.1
Coefficient thermal expansion	3.5×10^{-5} K^{-1}
Young's modulus	25 GPa
Poisson's ratio	0.2
Reservoir	
Reservoir temperature	190°C
Initial permeability $[X, Y, Z]$	10^{-15} m^2 (4×10^{-15} m^2)
Fracture	
Fractures per control volume, N	100
Max permeability multiplier	×60 (×400 : ×2)
Cohesion, S_0	2.7 MPa (0 MPa)
Static friction coef., μ_s	0.65
Dynamic friction coef., μ_d	0.55
Shear fracture stiffness, K_s	5×10^2 MPa m^{-1}

[1]Injection temperature was estimated from a Temperature/Pressure/Spinner-Flowmeter log collected after the 3.1 MPa stimulation.

3.3 Model setup

For both Desert Peak and Ngatamariki models, the computational domain is a 4×4×2 km cuboid with increasing resolution towards the central injection node. Fixed pressure boundary conditions on all sides allow water to flow out in response to injection; no additional heat flux is specified at the boundaries. Operation of other geothermal production or reinjection wells is not represented. The Desert Peak model is initialized with hydrostatic pressure and temperatures consistent with pre-stimulation conditions. Vertical gradients in the principal stress components are defined as an initial condition. Here, the principal stresses align with the Cartesian axes, i.e., $\sigma_x, \sigma_y, \sigma_z = \sigma_h, \sigma_H, \sigma_v$. The vertical stress gradient is given by density integration in the overburden. Horizontal stress gradients are specified as measured fractions of the vertical, e.g., σ_h=0.61σ_v for Desert Peak (Hickman and Davatzes, 2010).

A fixed overpressure is assigned to the centre node (1000 m depth). Injection of 100°C water proceeds at a rate proportional to local permeability and pressure gradients. Permeability changes with stress in accordance with the algorithm described in Section 3.1.

Model calibration proceeds as follows: (i) initial reservoir permeability is adjusted to match the initial injected flow rate for the fixed WHP; (ii) fracture cohesion is adjusted to match the onset time of injectivity gain; (iii) limiting fracture permeability is adjusted to match the magnitude of injectivity gain. Calibrated values of initial permeability, cohesion, and permeability gain, along with other material properties are given in Table 1. A sensitivity analysis of this calibration to model discretisation is given in (Kelkar et al., this volume).

The Ngatamariki model is a modified version of the Desert Peak model. Reservoir and injection temperature, injection depth and rock material properties likely differ to varying extents between Desert Peak and Ngatamariki. Nevertheless, we have opted to keep these constant between the two models as a control.

Our stated hypothesis is that n is intrinsically linked to damage zone geometry, which may in turn be linked to the distribution of fracture orientations. Therefore, the only changes for the Ngatamariki model are: (i) prescription of a more anisotropic fracture population (Fig. 2); and (ii) initial permeability, cohesion and permeability gain are recalibrated for a best fit to the data as outlined in Section 3.3.

4. RESULTS

4.1 First calibration

Matches between the calibrated Desert Peak and Ngatamariki models and the corresponding injectivity measurements are shown in Fig 3.

For Desert Peak, modelled injectivity evolution fits the data moderately well. Taking an onset time of 8 days, log-transformation and linear regression through the modelled injectivity curve (Fig 3C) suggest an injectivity exponent of n=0.4. However, the log-transformed data, plotted in Fig. 3C, suggests that an improved fit would result in an even lower exponent, probably around 0.3 – 0.35.

In contrast to the Desert Peak model, the best calibration achieved for the Ngatamariki model still provided a relatively poor match to the data. Injectivity gains are not matched at early time, injectivity increases too rapidly to overshoot the data before dropping off. Log analysis of the modelled curve suggests an injectivity exponent of n=0.35. This is significantly less than the 0.62 proposed by Grant et al. (2013).

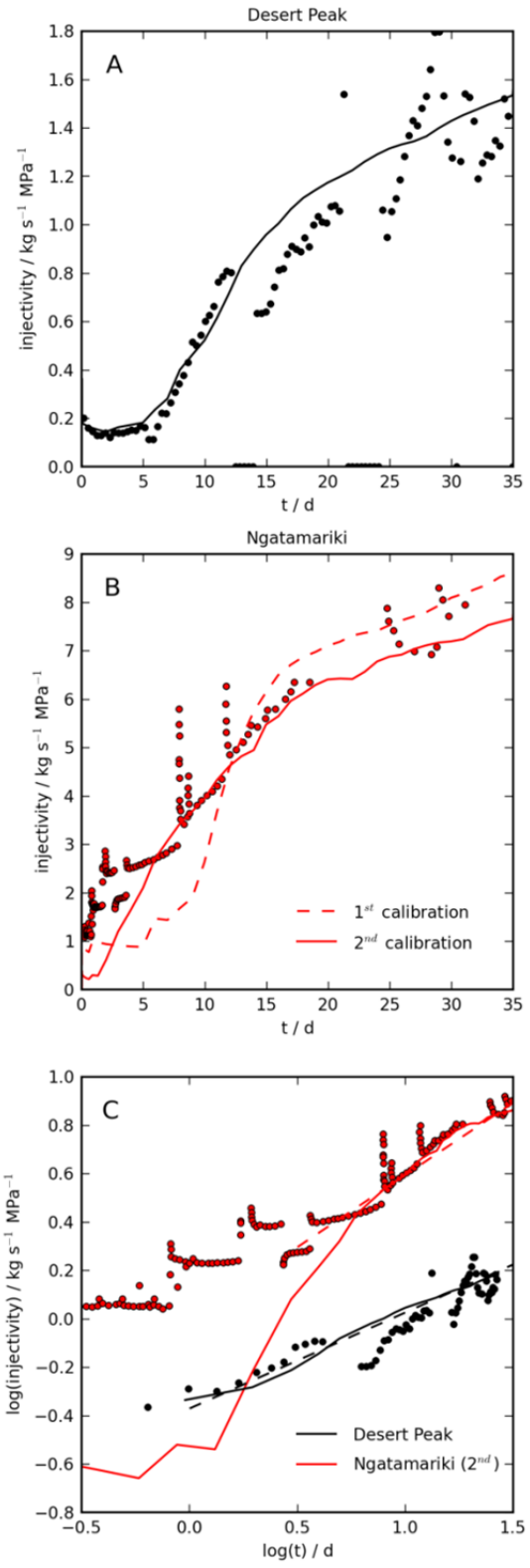

Figure 3: Injectivity data and model match for the Desert Peak (A) and Ngatamariki (B) stimulations. C. Log-transformed data with dashed lines showing straight-line fits to the modelled curves at late time.

This result indicates that prescribed anisotropy in the fracture orientation data (Fig. 2) is not sufficient to control injectivity behaviour (dashed line in Fig. 3B). In the next section, we investigate using more direct control over the damage zone geometry to modify the injectivity exponent. As a result of these findings, we obtain an improved calibration (solid line in Fig. 3C) of the Ngatamariki model (discussed in Section 4.3).

4.2 Sensitivity to damage zone geometry

The hypothesis tested here is that the geometry of the stimulated zone – spherical versus planar – affects the exponent of well injectivity change, n. To isolate and vary geometry only, we use a modified stress-permeability model that produces an ellipsoidal damage zone with a minor axis parallel to σ_h.

The permeability relationship described in Section 3.1 is modified so that only a single fracture is assigned to each control volume. The fracture normal is oriented parallel to σ_h - this provides the best accuracy in terms of resolving permeability anisotropy on a Cartesian mesh. The shear failure criterion is still assessed for this fracture orientation; however, arbitrary permeability increases are now specified parallel and perpendicular to the fracture – this provides control of the stimulation geometry. For example, if parallel and perpendicular modifiers are equal, an approximately spherical damage zone results. Higher degrees of anisotropy result in stimulated zones with more pronounced ellipsoidal geometry, which is quantified by the flattening along the σ_h axis. If the ellipsoid has major and minor axes r_H and r_h, then the flattening, f, is defined

$$f = \frac{r_H - r_h}{r_H}, \qquad (2)$$

so that f=0 for a sphere and f=1 for a planar circle. Here, r_H and r_h are defined to be parallel to σ_H and σ_h, and damage zone is arbitrarily delineated by the 160°C temperature isosurface (see Fig. 4).

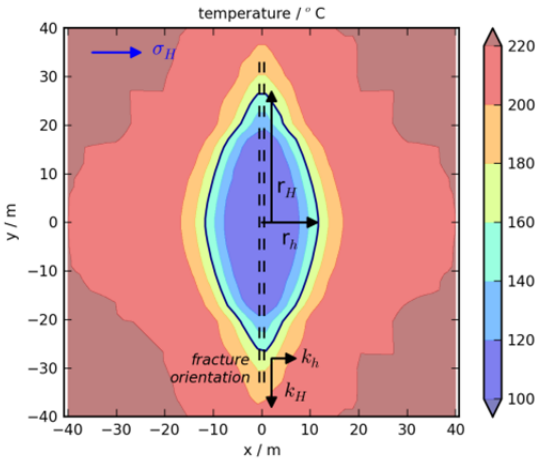

Figure 4: Conceptual model of a single fracture with anisotropic enhanced permeability (k_h, k_H). Temperature contours for a horizontal slice at 1000 m depth after 16 days of injection are overlaid. Measurement of r_h and r_H parameters from the 160°C temperature contour is indicated.

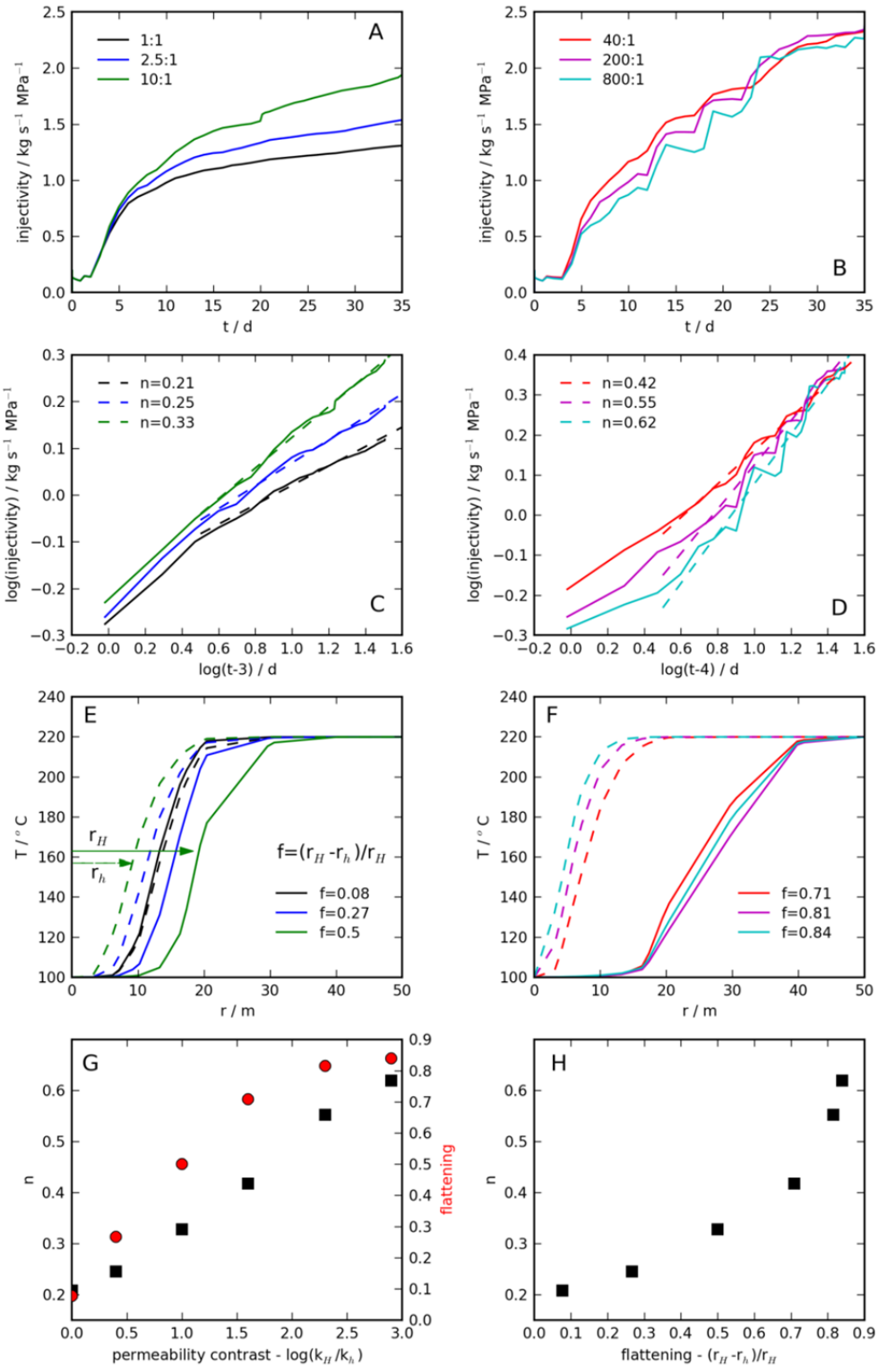

Figure 5: Injectivity response to various stimulation geometries. A-B. Injectivity evolution for six different fracture permeability anisotropies. The ratio of in-plane to out-of-plane stimulated fracture permeability is given in the legend. C-D. Log-transformed data after 3 days from A and after 4 days from B. Best fit straight lines are plotted with slopes given in the legend. E-F. Temperature profiles away from the injection point perpendicular to (dashed) and in the plane of the fracture (solid). Ellipsoid parameters r_h and r_H are measured at T=160° (shown for the green curves). The damage zone flattening is calculated and given in the legend. G. Dependence of injectivity exponent, n, (black squares) and damage zone flattening (red circles) on the permeability contrast of the stimulated fracture. H. Dependence of injectivity exponent, n, on damage zone geometry as parameterized by the flattening.

It is important to note that the concept of a single fracture is only invoked so as to implement permeability increase in the desired geometry. This does not imply that in practice a given stimulated volume is associated with a single fracture… although it may be. For instance, a spherical or moderately-ellipsoidal damage zone may arise from stimulation of many fractures of various orientations distributed throughout some volume. The analysis in this section focuses on the relationship between geometry and injectivity; not that between fracture distribution and geometry.

Figure 5 shows simulated injectivity behaviour for six different fracture permeability anisotropies; all other parameters are held constant. The anisotropy ranges from zero through to 800:1, i.e., in-plane fracture permeability increases 800 times more than out-of-plane.

In all cases, injectivity begins to rise after a period of three to four days. The injectivity curves are coincident for the first few days after which they begin to diverge, some dropping more rapidly than others. The shapes of the curves in Fig 5A (lower anisotropy) are more consistent with the Desert Peak data, while the curves in Fig 5B (higher anisotropy) look to provide a better match to the Ngatamariki data. Mesh effects are evident in the higher anisotropy simulations; this is due to extension of the elongated stimulated zone into lower resolution volumes of the mesh. However, these effects do not obscure the general trends and relationships discussed below.

For each simulation, the injectivity exponent, n, is obtained by log-transforming the data and fitting a straight line. Values range from 0.21 for the isotropic case up to 0.62 for the highest anisotropy. Furthermore, the exponent n appears to depend linearly on the logarithm of permeability anisotropy (see Fig. 5G).

The applied permeability anisotropy is here used as a tool to control the geometry of the stimulated zone and does not necessarily reflect that geometry itself. Instead, we use a geometric property of the ellipsoidal, 160°C (halfway between initial and injection temperatures) isosurface – a proxy for the cooled, damaged region – to quantify its shape. Fig. 5E-F shows the temperature profiles used to calculate the ellipsoidal flattening parameter (Eqn. (2)) for each simulation. In general, the flattening increases for the first 8 to 10 days of injection and stabilizes thereafter (Fig 6). Values quoted here are for 16 days after injection and vary from 0.08 for the isotropic case through to 0.84 for the highest anisotropy.

Flattening approaches a limiting value of 1 (as it must) with increasing anisotropy (Fig. 5G). This corresponds to the case of a planar stimulation zone, which is conceptually consistent with a single, large fracture or a narrow, confined aquifer. The latter structure was invoked by Grant et al. (2013) to derive analytical expressions for the injectivity exponent, n, which suggest between 0.5 and 1.5 depending on the nature of flow in stimulated aquifer. Consistent with this work, in Fig. 5H, we demonstrate n>0.6 for high-flattening, planar stimulation zones.

As the stimulated zone becomes more spherical, i.e., as flattening approaches 0, n decreases and approaches a lower value ~0.2. The monotonic relationship between n and flattening suggests that observations of well injectivity can be used to infer aspects of the stimulated volume. For instance, several stimulations at New Zealand geothermal fields exhibit injectivity gain at an exponent of n=0.6-0.7 (Grant et al., 2013); for these cases, our results suggest that primarily planar structures are being accessed. In contrast, injectivity gain at Desert Peak was consistent with n=0.3-0.4, and therefore a more spherical damage zone.

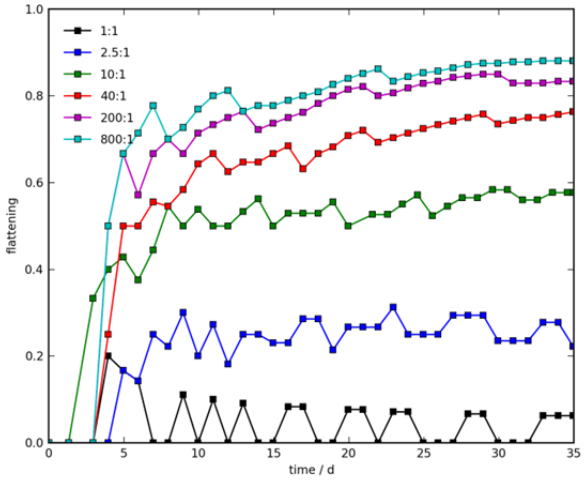

Figure 6: Flattening as a function of time for the six damage zone geometries investigated in Section 4.2.

4.3 Second calibration

Based on findings in the previous section, we have modified and recalibrated the Ngatamariki model. Use of a distributed fracture model for permeability enhancement yielded a value for n that was too low, despite a high degree of anisotropy in the orientation distribution (Fig. 3B). Thus, the model was modified to use the single-fracture with prescribed permeability anisotropy relationship.

Subsequent recalibration of the model yielded the injectivity behaviour shown by the solid curve in Fig. 3B. Injectivity is now significantly underestimated at early time; however, the match after 3 to 4 days is much improved.

Log-analysis of the injectivity curve for the modified model indicates a value for n of 0.60 at late time, corresponding to a flattening parameter of 0.79. This suggests a flatter, more elongated stimulation zone and indicates that stimulation at Ngatamariki occurred within a single fracture or confined aquifer, rather than on a distributed, albeit anisotropic, fracture mesh.

5. CONCLUSION

We have extended the previously-developed Desert Peak shear-stimulation model to describe thermal stimulation of a well at Ngatamariki. The Ngatamariki well differs in several respects, exhibiting both a higher initial flow rate and exponent of injectivity evolution, n. To achieve a reasonable match to the higher value of n, a modified stress-permeability relationship was implemented. Calibration of the in- and out-of-plane permeability components of a single stimulated fracture yielded an exponent of 0.60. The resulting damage zone was relatively planar (flattening of 0.79) indicating stimulation was occurring within a narrow fracture zone.

This result is consistent with the broader finding of this work: that the injectivity exponent reflects the geometry of the stimulated region. One end-member is the spherical, isotropic damage zone associated with a lower exponent (n = 0.3-0.4); in the case of Desert Peak, this geometry is probably linked to stimulation of a distributed fracture mesh with low orientation bias. In contrast, Ngatamariki is a fine example of the other end-member: a high injectivity exponent (n = 0.62) linked to a planar stimulation zone, which is perhaps correlated with a single fracture or confined aquifer. However, while a link between geometry and injectivity has been established in these numerical experiments, proper confirmation of our hypothesis would require either in-situ observation or indirect measurement (e.g., distribution of microseismicity, changes in resistivity) of the cooled volume.

The geometry of the stimulated region has important implications for operation of both natural and enhanced geothermal systems (EGS). For example, a flat planer volume extending further from the wellbore may be more useful when the goal of the stimulation is to establish a connection between an outlier well and the main producing regions, as was the case of the Desert Peak EGS project. On the other hand, a spherical stimulated volume may be more efficient for maximizing heat extraction from a given volume. Furthermore, a spherical volume offers the best chance of intersecting a pre-existing permeable feature if the relative location to the well is unknown.

Given the potential benefits of controlling stimulation geometry, a natural extension of this work would be to investigate, for given formation properties (e.g., fracture distribution, material properties), the effects, if any, of injection pressure and temperature. That is, is the stimulation geometry predetermined by intrinsic reservoir properties, or can it be controlled to some extent by operations at the surface? This question will be addressed in future research.

ACKNOWLEDGEMENTS

Funding for this work was provided by US DOE Office of Geothermal Technologies under Work Authorization No. GT-100036-12_Revision 1. The coupled flow and stress numerical simulation capabilities in FEHM applied for this work were done at LANL under the Zero Emission Research & Technology (ZERT-II) project funded by US DOE through its CO_2 sequestration R&D program. Mighty River Power for Ngatamariki field data.

REFERENCES

Chabora, E., Zemach, E., Spielman, P., Drakos, P., Hickman, S., Lutz, S., Boyle, K., Falconer, A., Robertson-Tait, A., Davatzes, N. C., Rose, P., Majer, E., Jarpe, S.: Hydraulic Stimulation of Well 27-15, Desert Peak Geothermal Field, Nevada USA. *Proc. 37th Stanford Geotherm. Workshop.* (2012).

Davatzes, N. C., Hickman, S. H.: Fractures, Stress and Fluid Flow Prior to Stimulation of Well 27-15, Desert Peak, Nevada, EGS Project. *Proc. 34th Stanford Geotherm. Workshop*. (2009).

Dempsey, D., Kelkar, S., Lewis, K., Hickman, S., Davatzes, N., Moos, D., Zemach, E.: Modeling Shear Stimulation of the Desert Peak EGS Well 27-15 Using a Coupled Thermal-Hydrological-Mechanical Simulator. *Proc. 47th US Rock Mech. Symp.* (2013).

Faulds, J. E., Coolbaugh, M. F., Benoit, D., Oppliger, G., Perkins, M., Moeck, I., Drakos, P.: Structural Controls on Geothermal Activity in the Northern Hot Springs Mountains, Western Nevada: The Tale of Three Geothermal Systems (Brady's, Desert Peak and Desert Queen). *GRC Transac.*. v. 34, pp. 675-683. (2010).

Grant, M, A., Clearwater, J., Quinao, J., Bixley, P. F., Le Brun, M.: Thermal Stimulation of Geothermal Wells: A Review of Field Data. *Proc. 38th Stanford Geotherm. Workshop*. (2013).

Halwa, H., Wallis, I. C., Torres Lozada, G.: Geological Analysis of the Volcanic Subsurface using Resistivity-Type Borehole Images in the Ngatamariki Geothermal Field, New Zealand, *This Volume*. (2013)

Hickman, S. H., Davatzes, N. C.: In-situ Stress and Fracture Characterization For Planning of an EGS Stimulation in the Desert Peak Geothermal Field, Nevada. *Proc. 35th Stanford Geotherm. Workshop.* (2010).

Kelkar, S., Dempsey, D., Zyvoloski, G., Clearwater, J., Wallis, I., and Pogacnik, J.: Investigation of mesh sensitivity in coupled thermal-hydrological-mechanical models: Examples from Desert Peak, Nevada, USA and Ngatamariki, New Zealand. *This Volume.* (2013)

Lee, H. S., Cho., T. F.: Hydraulic Characteristics of Rough Fractures in Linear Flow under Normal and Shear Load. *Rock Mech. Rock Engng.* v. 35, pp. 299-318. (2002).

Lutz, S. J., Hickman, S. H., Davatzes, N. C., Zemach, E., Drakos, P., Robertson-Tait., A.: Rock Mechanical Testing and Petrologic Analysis in Support of Well Stimulation Activities at the Desert Peak Geothermal Field, Nevada. *Proc 35th Stanford Geotherm. Workshop.* (2010).

Rowland, J. V., Sibson, R., H.: Structural controls on hydrothermal flow in a segmented rift system, Taupo Volcanic Zone, New Zealand. *Geofluids*, v. 4, pp.259-283. (2004).

Zyvoloski, G. A.: FEHM: A control volume finite element code for simulating subsurface multi-phase multi-fluid heat and mass transfer. *LANL Doc. LAUR-07-3359*. Los Alamos, NM. (2007)